The Astronomical Journal, 146:5 (8pp), 2013 July doi:10.1088/0004-6256/146/1/5

THE CATALOG OF POSITIONS OF OPTICALLY BRIGHT EXTRAGALACTIC RADIO SOURCES OBRS–2

L. Petrov
Astrogeo Center, Falls Church, VA 22043, USA; Leonid.Petrov@lpetrov.net
Received 2013 January 23; accepted 2013 April 4; published 2013 June 4

ABSTRACT

Future space-borne astrometry missions, such as *Gaia*, will be able to determine the optical positions of hundreds of quasars with submilliarcsecond accuracies comparable to those achieved in radio by very long baseline interferometry (VLBI). Comparisons of coordinate systems from space-borne missions and VLBI will be very important, first for investigations of possible systematic errors and second for investigations of possible shifts between centroids of radio and optical emissions in active galactic nuclei. In order to make such a comparison more robust, a program for densification of the grid of radio sources detectable with both VLBI and *Gaia* was launched in 2006. Program sources are 398 quasars with declinations $>-10^\circ$ that are brighter than 18 mag at the *V* band. The first two observing campaigns were run in 2007–2008. In the third campaign, a set of 291 objects from that list was observed with the VLBA+EVN in 2010–2011 with the primary goal of producing their images with milliarcsecond resolution. In this paper, following the method of absolute astrometry, coordinates of observed sources have been derived with milliarcsecond accuracies from analysis of these observations. The catalog of positions of 295 target sources, estimates of their correlated flux densities at 2.2 and 8.4 GHz, and their images are presented. The accuracies of source coordinates are in a range of 2–200 mas, with a median of 3.2 mas.

Key words: astrometry – catalogs – surveys

Online-only material: color figures, machine-readable and VO tables, supplemental data (tar.gz)

1. INTRODUCTION

Nowadays, the most precise method for deriving source positions is very long baseline interferometry (VLBI), first proposed by Matveenko et al. (1965). Starting in 1971, when the first catalog of source positions determined with VLBI was published (Cohen & Shaffer 1971), continuous efforts have been undertaken to increase the number of compact sources with positions known at a nanoradian level, reducing their position systematic errors and improving the sky coverage. By 2012, the number of sources with positions determined by VLBI under absolute astrometry and geodesy programs[1] reached 7215. Using absolute VLBI astrometry[2] (L. Petrov, in preparation) and differential VLBI astrometry (A. Deller et al. 2013, in preparation), ongoing efforts for densification of the catalog of positions of compact radio sources promise to double the number of such sources within several years.

As part of the densification of the catalog of compact radio sources, the program for observing quasars and BL Lac objects that are 18 mag or brighter at the *V* band and sufficiently strong in radio was launched in 2006 (Bourda et al. 2008) with the eventual goal of highly accurately deriving their position from VLBI observations in the absolute astrometry mode. The motivation of this program is to increase the number of sources whose positions can be determined both with VLBI and the space-borne mission *Gaia* (Lindegren et al. 2008), scheduled to be launched in 2013. After reducing VLBI positions for offsets caused by a misalignment of centers of radio and optic images and for a frequency-dependent core shift (Kovalev et al. 2008; Porcas 2009; Sokolovsky et al. 2011), the systematic differences between radio and optical positions will be thoroughly investigated. Since position catalogs produced with VLBI and *Gaia* will be completely independent, investigation of systematic differences will be very important for the assessment of the overall quality of *Gaia* results and, possibly, for identification of errors in the VLBI position catalog.

The detailed observing scheme of this project is presented in Bourda et al. (2008). The source selection strategy is introduced in Charlot et al. (2007). The original observing sample consisted of 447 optically bright, relatively weak extragalactic radio sources associated with quasars or BL Lac objects from the Veron-Cetty & Veron (2010) catalog with declinations above -10°. Hereafter, I will not distinguish between BL Lac objects and quasars, and I will call all these objects quasars. The first VLBI observing campaign in 2007 resulted in the detection of 398 targets with the European VLBI Network (EVN; Bourda et al. 2010), although no attempt to generate their images or derive their positions was made. During the second observing campaign, a subset of 105 sources detected in the previous campaign was observed with the global VLBI network which comprises the Very Long Baseline Array (VLBA) and EVN observing stations. This campaign had the goal of revealing the source morphology on milliarcsecond scales from VLBI images (Bourda et al. 2011) for consecutive screening of the objects with a structure that may potentially cause non-negligible systematic position errors. Their positions were derived by Petrov (2011) and formed the OBRS–1 catalog.

In 2010–2011, the remaining 291 sources were observed in the third campaign, hereafter called OBRS–2, with the global network that comprises the VLBA and EVN observing stations in a mode similar to the second campaign. Here, I present the results of a data analysis of these observations. The observations and their analysis are described in Sections 2 and 3. The position catalog is presented in Section 4 and discussed in Section 5. Concluding remarks are given in Section 6.

2. OBSERVATIONS

During the OBRS–2 campaign, there were three observing sessions with 10 VLBA stations and 5–6 EVN stations from

[1] See http://astrogeo.org/rfc
[2] See http://astrogeo.org/vcs7

Table 1
Summary of Observing Sessions

Epoch of Observing Session	Session ID	Session Duration[a] (hr)	Number of Program Sources
2010 Mar 23	gc034a	48	97
2011 Nov 8	gc034bcd	58	118
2011 Mar 15	gc034ef	40	77

Note. [a] Excludes maintenance gaps.

this list: EFLSBERG, MEDICINA, ONSALA60, YEBES40M, DSS63, HARTRAO, and NOTO. The first four EVN stations participated in every experiment, while the three remaining stations participated in some experiments. Each program source was observed in one session, in three to four scans, each five minutes long. Two sources, 1148+387 and 1203+109, were observed in two sessions in five scans. In addition to 291 program sources, eight strong calibrators were also observed.

A summary of the observing sessions is given in Table 1. Observations were made at *X* and *S* bands simultaneously. Data were sampled with 2 bits per sample at the aggregate rate of 512 Mbit s^{-1}. The intermediate frequencies were selected to provide continuous bandwidths, [8.37699, 8.44099] and [2.22699, 2.29099] GHz. Such a setup is not favorable for astrometry. Spanning frequencies over 500 MHz, as is done in all other dual-band absolute astrometry VLBA surveys, improves the precision of group delay determination and, therefore, source position precision *by one order of magnitude*. The position accuracy of sources observed with a wide-band frequency setup and detected at 3000–8000 km long baselines is limited by systematic errors. The position accuracy of sources observed in a single frequency band spanning over 64 MHz is limited by thermal noise.

The second limitation of the OBRS–2 schedule for the astrometry used is a relatively rare observation of sources at low and high elevations for a better estimation of the troposphere path delay in the zenith direction, which increases systematic errors. The VCS1 survey (Beasley et al. 2002) suffered a similar deficiency in design, and analysis revealed systematic errors at a level of 0.4–0.5 mas. We can assume that systematic errors of OBRS–2 were at a similar level. Though since the contribution of the thermal noise in the error budget of OBRS–2 experiments is one order of magnitude higher than in VCS experiments, these increased systematic errors did not cause further noticeable accuracy degradation.

Of 291 program objects, 58 sources were observed and detected in other absolute astrometry programs such as the VLBA Calibrator Survey (Beasley et al. 2002; Fomalont et al. 2003; Petrov et al. 2005, 2006; Kovalev et al. 2007; Petrov et al. 2007), regular VLBA geodetic observations (Petrov et al. 2009; Pushkarev & Kovalev 2012), and ongoing VLBI observations of Two Micron All Sky Survey galaxies (Condon et al. 2011). Positions of all but four sources, 0106+315, 0809+483, 1213+097, and 2247+140, are known with accuracies better than 0.4 mas. These 54 program sources and 8 calibrators provided a sufficient overlap for tying position estimates to the existing catalog and for evaluation of position accuracy.

3. DATA ANALYSIS

The data were correlated with the DiFX software correlator (Deller et al. 2011) at the National Radio Astronomy Observatory. The correlator computed the spectrum of cross-correlation and autocorrelation functions with a frequency resolution of 0.25 MHz at accumulation intervals of 1 s long.

3.1. Preliminary Analysis

The procedure of further analysis is described in full detail in Petrov et al. (2011a). I present here only a brief outline. First, log files are parsed, system temperature and phase calibration are analyzed, and points with outliers are removed. No phase calibration signal for non-VLBA stations was recovered due to a DiFX correlator limitation (which was lifted later in 2011). Next, the fringe amplitudes were corrected because of a distortion in the sampler due to digitization. Then, the fringe amplitudes were multiplied by the a priori System Equivalent Flux Density (SEFD) $\sqrt{(g_1\, g_2 / T_{\rm sys1}\, T_{\rm sys2})}$, where g_i and $T_{\rm sys,i}$ are the elevation-dependent gain and system temperature of the ith antenna, respectively. Next, a phase delay rate, group delay, group delay rate, and fringe phase of every observation were determined for each baseline at *X* and *S* bands separately using the wide-band fringe-fitting procedure. These estimates maximize the amplitude of the cross-correlation spectrum coherently averaged over all frequency channels in all intermediate frequencies of a band and over all accumulation periods of a scan. Hereafter, I call these "observables" derived for a given baseline, for a given interval of time, when the antennas were observing on-source. After the first run of fringe fitting, 12 observations at each baseline with a reference station with the strongest signal-to-noise ratios (S/Ns) were used to adjust the station-based complex bandpass corrections, and the fringe-fitting procedure with the bandpasses applied was repeated. The part of analysis described above is done with $\mathcal{PIMA}$ software.[3]

Further analysis was split into two routes: astrometric and imaging. Following the astrometric route, total group delays and phase delay rates were computed on a common fringe reference time epoch within a scan, using results of fringe fitting. These observables, along with auxiliary information describing observations, were exported to the VTD/post-Solve VLBI analysis software[4] for interactive analysis. Initially, only observables with a high S/N were chosen to ensure that the probability of false detection was less than 0.001. This S/N threshold is 5.8 for OBRS–2 experiments. A detailed description of the method for evaluation of the probability of false detection can be found in Petrov et al. (2011a).

Then, theoretical path delays as well as their partial derivatives were computed according to the state-of-the-art model (Petrov et al. 2009). Differences between observed group delays and theoretical path delays were used for estimation of corrections to a parametric model that describes the perturbation of the theoretical model using least squares (LSQ). The parametric model included coordinates of target sources and a number of nuisance parameters that model station positions, Earth orientation parameters, clock, and atmosphere path delay. The initial solution was made using *X*-band group delay and repeated using *S*-band delays.

The data set was cleaned for outliers, i.e., observations with residual group delays exceeding 5σ. The most common reasons for an observation to have a large residual are a failure of the fringe-fitting procedure to find the main maximum, the presence of radio interference, and false detection. Simultaneous solving

[3] Available at http://astrogeo.org/pima.
[4] Available at http://astrogeo.org/vtd.

for source positions with only few detections in the presence of outliers poses a certain risk. One bad observation may corrupt the solution, and as a result, remaining good observations of that source may get high residuals and the outlier elimination procedure may discard them. Identifying that bad observation(s) often required several trials. When the data set was cleaned, I gradually lowered the S/N limit from 5.8 to 5.0 with a step of 0.1. The status of all observations with an S/N < 5.8 was initially set to "suppressed." That means these observations did not contribute to estimation of the parametric model, but the parametric model evaluated at the previous step was applied for computing their residuals. Suppressed observations with residuals by modulo less than 5σ at the *S* band and less than 4σ at the *X* band were restored one by one, starting with the smallest normalized residual. After flipping the status "suppressed," the LSQ solution was updated for including this observation into the parameter estimation model, and the process was repeated. There was a significant fraction of false detections with an S/N < 5.8. But such observations have random group delay estimates uniformly distributed over a 4μs-wide search window. The probability that the group delay from a false detection will have a residual within 2–5 ns of the expected value, and therefore may be identified as a good observation, is on the order of $(1–2) \times 10^{-3}$. Suppression of observations with huge residual delay rates (several such points were found) reduces this probability even further.

Then the fringe-fitting procedure was repeated with a narrow fringe search window for those points that were marked as outliers. The center of the fringe search window over delay and delay rate were set to the expected value of the delay and delay rate computed as a sum of the a priori delay or delay rate and the contribution from the parametric model derived during the LSQ adjustment. The width of the search window was set to 5 ns for the *S* band and 3 ns for the *X* band. In addition to that, I re-ran the fringe-fitting procedure with the updated a priori model for all the sources that have position adjustments exceeding $1''$. For instance, 0744+092 had the a priori position $4''.8$ off the VLBI position. When a source has a large position error, a nonlinear fringe phase change over a scan of 300 s long becomes significant and causes noticeable de-correlation.

The interactive analysis procedure was repeated with the updated results of the fringe fitting. The S/N threshold was lowered to 4.8 because the probability of false detection is less for a narrow fringe search window. The outlier elimination procedure was repeated. Baseline-dependent additive weight corrections were computed in such a way as the ratio of the weighted sum of post-fit residuals to their mathematical expectation was close to unity. This computation procedure is described in full detail by Petrov et al. (2009).

3.2. Multiple Sources

Careful analysis revealed five sources in which more than 15% of S/Ns > 5.8 marked as outliers were not diagnosed as radio interference or errors in fringe fitting. These sources had different positions derived from *X*- and *S*-band group delays. If we invert the suppression status of points for these sources, i.e., restore a point that was suppressed and suppress the point that was used in the solution, and re-run the procedure of outlier elimination, then we can get a position that is consistent with one at the opposite band. These phenomena can be explained if we suggest that a source has multiple components separated at an arcsecond level, strong enough to be detected. I used the following technique for component separation in order to investigate these sources. I cloned visibilities of these sources and treated them as different objects with different positions. Using their preliminary positions as a priori, I shifted phases of visibilities to the new positions and performed the fringe search in a narrow window, the same way I treated outliers. This approach yielded a significant number of new detections for both components at one or both bands. New detections confirmed the hypothesis that a source is multiple. In the following analysis, components of multiple objects are treated as different sources.

3.3. Global Astrometric Solution

The result of the interactive solution provided a clean data set of *X*- and *S*-band group delays with updated weights. The data set that was used for the final parameter estimation utilized all dual-band *S*/*X* data acquired under the absolute astrometry and space geodesy programs from 1980 April through 2012 December, including 76,079 observations from OBRS–2 experiments, for a total of 8.89 million observations. Among program sources, 58 common objects were observed in other absolute astrometry VLBI experiments. I made four solutions. The first three solutions used the global data set, except for observations of 58 common objects, and observables from the OBRS–2 experiments: the first solution used the *X*-band group delays, the second solution used the *S*-band group delays, and the third solution used the ionosphere free linear combinations of *X*- and *S*-band group delays. The fourth reference solution used all experiments in the global data set with only the exception of OBRS–2 data.

OBRS–2 experiments were analyzed exactly the same way as 5497 other VLBI observing sessions, using the same analysis strategy that was used for processing prior observations for the ICRF (Ma et al. 1998), VCS, VGaPS, Long Baseline Array Calibrator Survey (LCS; Petrov et al. 2011b), and K/Q survey (Lanyi et al. 2010) catalogs. Positions of all the sources were adjusted in a single gigantic LSQ solution, together with more than one million nuisance parameters and by applying minimal constraints. Detailed description of the analysis procedure can be found in Petrov (2011).

It should be noted that source coordinates cannot be derived *only* from observations. The equation of light propagation that relates source coordinates with observed group delays is invariant with respect to a group of rotational and translational transformations. A family of solutions satisfies the equation. In order to pick a specific element from this family, I applied the no-net rotation constraints on the positions of 212 sources marked as "defining" in the ICRF catalog that required the positions of these sources in the new catalog to have no rotation with respect to their positions in the ICRF catalog. No-net rotation and no-net-translation constraints on site positions and linear velocities were also applied. The specific choice of identifying constraints was made to preserve the continuity of the new catalog with other VLBI solutions made during the last 15 years, including but not limited to such catalogs as ICRF2, KQ (Lanyi et al. 2010), LCS1 (Petrov et al. 2011b), and others.

3.4. Image Analysis

The same data set of visibilities was used for source imaging. At first, I discarded all visibilities from observations that were marked as outliers in the final step of the interactive analysis procedure. Next, the data were averaged over time and frequency after phase rotation for the contribution of group

delay, group delay rate, and phase delay rate found by the fringe search procedure. Since the fringe-fitting procedure was baseline-based, the baseline-dependent parameters of fringe fitting should be transformed to station-based parameters in order to preserve phase closures of visibilities. This transformation was done separately for the visibilities of each scan, each subarray, and each band. Although the experiments were scheduled for all the stations of the network to observe the same source during scan time, it may happen that some sources were detected only at a subset of baselines that do not have common stations. For each scan, I found a scan-reference time as a weighted mean epoch of the observations used. I selected a reference station for each subarray and solved with least squares for station-dependent group delays, group delay rates, and phase delays using baseline-dependent estimates of these quantities found by the fringe search procedure as the right-hand side of equations that relate baseline-dependent and station-dependent observables. These station-dependent quantities related to a common epoch within a scan were used to phase rotate the visibilities. After phase rotation, the visibilities were averaged over 32 spectral channels in each intermediate frequency and over 4 s intervals.

The averaged visibilities and accompanying weights were split into sources and written in separate files. Further processing was done using the DIFMAP software package (Shepherd 1997), and I used the automatic imaging procedure muppet developed by Martin Shepherd and Greg Taylor (Pearson et al. 1994; Taylor et al. 1996) that started from a point-source model as an initial guess and performed a sequence of image cleaning and phase and amplitude self-calibrations with and without taper.

I developed a web application that allowed me to inspect images visually and flag those that showed visible artifacts. Of 564 images made automatically, 63 were flagged, and I reprocessed them interactively. These were the sources that either had points with amplitude outliers that an automatic procedure was unable to flag or sources with too few observations, in a range of 15–35, when an automatic procedure of hybrid imaging becomes unstable. In total, images were produced for 279 sources at the *X* band and for 285 sources at the *S* band.[5] As a measure of source strength, I derived two quantities from source brightness distributions: I computed the median-correlated flux densities at baselines with projection lengths shorter than 900 km and longer than 5000 km.

Some weak sources have too few points for successful imaging. In order to provide a measure of source strength at long and short baselines for these objects, I made a simplified amplitude analysis similar to what was done in processing OBRS–1 observations. I used averaged corrections to gains evaluated during self-calibration of strong sources and applied these corrections to the a priori SEFDs. From fringe amplitudes calibrated this way, I computed the median-correlated flux densities at baselines with projection lengths shorter than 900 km and longer than 5000 km, similar to what I did in image processing. In order to check this simplified method, I processed some strong sources as well and compared their median-correlated flux densities derived by a rigorous imaging procedure. The disagreement did not exceed a level of 15%.

Detailed analysis of produced images is beyond the scope of this paper and will be given in the future in a separate publication (G. Bourda et al. 2013, in preparation).

[5] Images in FITS format as well as calibrated visibilities are available at http://astrogeo.org/obrs.

4. RESULTS

I have detected at one band all but one source 0843−025 (J0845−0241). In this paper, objects with multiple components are treated as different sources, although most likely these are parts of the same objects.

Since 58 of 295 detected sources have been observed with VLBA in different programs at the *X* band in a wide-band mode with frequency spanned over 494 and 992 MHz, their position uncertainties are a factor of 10–20 better than the position uncertainties from OBRS–2 experiments with the same S/N and the same number of observables. Therefore, for the purpose of comparison with the OBRS–2 catalog, positions of these sources can be considered to be precisely known. I excluded from comparison four sources that are resolved and had uncertainties exceeding 0.4 mas in the reference solution.

A comparison showed that the solution that used ionosphere-free linear combinations of X/S group delay observables did not improve the agreement between position estimates of 54 common sources over the solution that used *X*-band-only observables. The position uncertainties of OBRS–2 observations are too large for the residual ionosphere contributions to affect positions at a significant level. I computed the variance, which, when added in quadrature to source position uncertainties, makes the ratio of the sum of weighted squares of position differences to their mathematical expectations close to unity. These variances are 1.7 mas in right ascension and 2.1 mas in declination for the *X*-band solution, and 2.1 mas in right ascension and 2.4 mas in declination for the *S*-band solution.

4.1. OBRS–2 Catalog

The majority of sources were detected at both bands, and there are position estimates from two solutions that used *X*-band and *S*-band observables from the OBRS–2 experiments. Preference was given to the solution that used *X*-band observables because the detection limit at the *X* band was lower and the contribution of the residual ionosphere after applying a reduction for the total electron contents from GPS observations at the *X* band is one order of magnitude less than at the *S* band. If the reweighted position uncertainty from the *S*-band solution was at least a factor of 1.5 smaller than the uncertainty from the *X*-band solution, then the position from the *S*-band solution was used in the final catalog. Although there are additional, more precise observations of 58 common sources in other absolute astrometry experiments, these observations were excluded in solutions 1 and 2 in deriving the OBRS–2 catalog.

The positions of 295 sources observed in the OBRS–2 experiment are listed in Table 2. The first and second columns provide the IVS source name (B1950 notation) and IAU name (J2000 notation). The third and fourth columns give source coordinates at the equinox on the J2000 epoch. Columns 5 and 6 give reweighted source position uncertainties in right ascension and declination in mas (without $\cos\delta$ factor), and Column 7 gives the correlation coefficient between the errors in right ascension and declination. Column 8 shows the band ID of the solution that was used to derive position of a given source. The number of group delays used in the analysis is listed in Columns 9 and 10. Columns 11 and 12 provide the median value of the correlated flux density in Jansky at the *S* band at baseline projection lengths shorter than 900 km and longer than 5000 km. The latter estimate serves as a measure of the correlated flux density of an unresolved source component.

Table 2
The OBRS–2 Source Position Catalog

IAU Name		Source Coordinates		Position Errors				No. of pnt		F_{corr} S Band		F_{corr} X Band		Flags	
B1950	J2000	α (h m s)	δ (° ′ ″)	σ_α (mas)	σ_δ (mas)	Corr	Band	S	X	Short (Jy)	Unresolved (Jy)	Short (Jy)	Unresolved (Jy)	S	X
J0001+0632	2358+062	00 01 23.694601	+06 32 30.93754	3.52	15.24	−0.811	X	38	31	0.018	0.022	0.018	0.008	m	m
J0005+1609	0003+158	00 05 59.237650	+16 09 49.02157	1.86	2.53	−0.342	X	168	168	0.143	0.070	0.196	0.057	m	m
J0015+3052	0012+305	00 15 36.022281	+30 52 29.79522	2.98	7.35	−0.437	X	12	32	0.026	0.015	0.017	0.006		m
J0017+1451	0015+145	00 17 36.903866	+14 51 01.88067	1.92	3.10	−0.557	X	164	166	0.065	0.039	0.053	0.030	m	m
J0027+4514	0025+449	00 27 42.262713	+45 14 57.07879	2.72	2.88	−0.477	X	222	129	0.048	0.042	0.024	0.015	m	m
J0035+1553	0033+156	00 35 55.537977	+15 53 16.45642	23.81	23.11	−0.267	S	29	3	0.074	<0.017	−1.00	−1.00	m	
J0037+3938	0034+393	00 37 36.725767	+39 38 11.79014	2.44	2.86	−0.354	X	210	121	0.142	0.044	0.039	0.012	m	m
J0041−0143	0038−019	00 41 26.008767	−01 43 15.67847	2.03	5.16	−0.625	X	143	125	0.056	0.049	0.037	0.032	m	m

Notes. Units of right ascension are hours, minutes, and seconds. Units of declination are degrees, minutes, and seconds.

(This table is available in its entirety in machine-readable and Virtual Observatory (VO) forms in the online journal. A portion is shown here for guidance regarding its form and content.)

Columns 13 and 14 provide the median of the correlated flux density at the *X* band at baselines shorter than 900 km and longer than 5000 km. If no information about correlated flux density is available, −1.000 is used as a placeholder. The last two columns note if an image is available for the *S* or the *X* band: "m" if available, blank if not.

The semi-major axes of error ellipses range from 2.1 to 200 mas, with the median 3.2 mas, and for 80% sources the position errors are under 5.2 mas. The major factor that results in position uncertainty exceeding 5 mas is a lack of detections at long baselines. Sources with large position uncertainties are either highly resolved or very weak moderately resolved objects.

4.2. Analysis of Multiple Sources

I found Very Large Array (VLA) images of all multiple sources detected in the OBRS–2 campaign in the NRAO archive.[6]

0154+31A/0154+31B has two components 2.″592 apart. Component A is compact and was detected at the 5 mJy level at the *X* band at intercontinental baselines with Effelsberg. It was not detected at intercontinental baselines at the *S* band. Since the sensitivity of baselines with Effelsberg is a factor of 4–5 worse at the *S* band than at the *X* band, this can be explained if a source has a spectral index flatter than −1.1 ($S \sim f^{\alpha}$). Component B is stronger at the *S* band, but has only three detections at the 5 mJy level at the *X* band at short baselines only. Cross-matching against *Wide-field Infrared Survey Explorer* (*WISE*) infra-red catalog of point sources (Wright et al. 2010) revealed a WISE J015715.32+315419.2 object with magnitude 13.9 at 3.6 μ within 0.″36 of 0154+31A. Weak emission between components A and B visible at the VLA image (Figure 1) suggests that components B and C are radio lobes, and component A is the core.

0809+483/0809+48B/0809+48C has three components within 6″. Components B and C coincide with extended radio lobes visible at the VLA image (Figure 2). Compact component A with *X*-band flux density 5 mJy at intercontinental baselines is located between radio lobes. WISE J081336.05+481302.7 with magnitude 13.5 at 3.6 μ was found within 0.″11 of component A.

1323+65A/1323+65B has two components with separation 3.″157. Although component B is five times stronger at the *X* band at the VLA image (Figure 3) than component A—21 mJy versus 4 mJy—it is not detected at VLBA scale at the *X* band. Component A with correlated flux density 4 mJy at intercontinental baselines lies within 0.″20 of WISE J132529.70+651513.3, which has magnitude 14.6 at 3.6 μ.

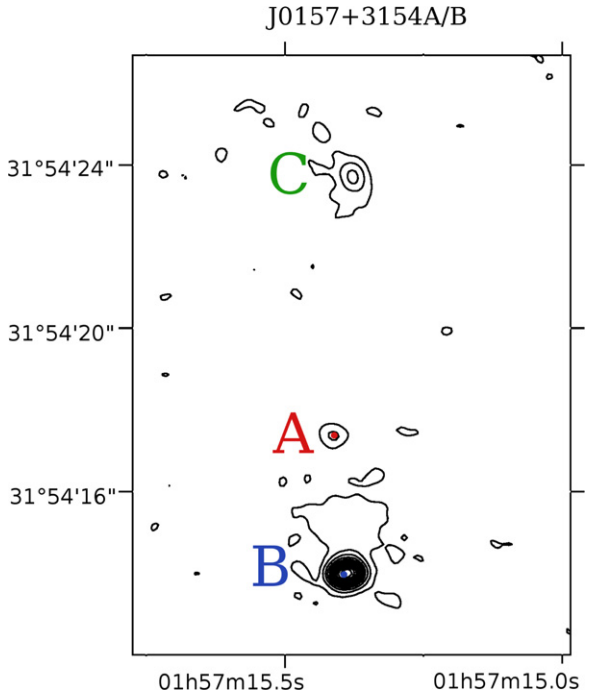

Figure 1. VLA image of double source 0154+31A/0154+31B at 8.44 GHz on epoch 1991 July 24 with beam size 0.″30, project AB611 (MITVLA), is shown as a contour map. VLBI positions are shown with filled circles. Component A is the most compact and has a flux density of 4 mJy at intercontinental baselines, the same as at the 27 km long VLA baselines. Component B is resolved and visible only at short baselines.

(A color version of this figure is available in the online journal.)

1335−06A/1335−06B has two components 4.″896 apart. Component B, associated with a radio lobe (Figure 4), was detected at the *S* band only. Compact component A with flux density 7 mJy at the *X* band is within of 0.″18 of WISE J133807.98−062711.0, which has magnitude 13.9 at 3.6 μ.

1340+60A/1340+60B has two components separated at 3.″014. The source looks elongated in the VLA image at 1.4 GHz (Figure 5). Component B was detected at the *S* band only.

[6] https://archive.nrao.edu

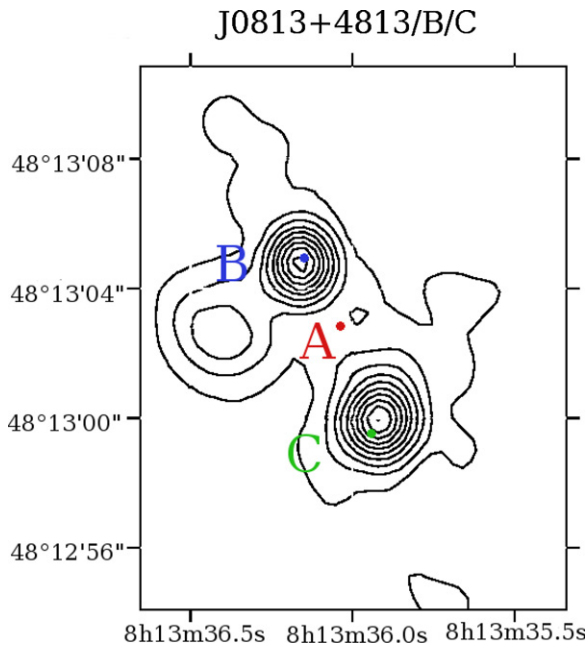

Figure 2. VLA image of triple source 0809+483/0809+48B/0809+48C at 4.86 GHz on epoch 1995 October 15 with beam size 1.″27, project AS561, is shown as a contour map. VLBI positions are shown with filled circles. Component A is the most compact and has a flux density of 5 mJy at intercontinental baselines. Components B and C are resolved and visible only at short baselines.

(A color version of this figure is available in the online journal.)

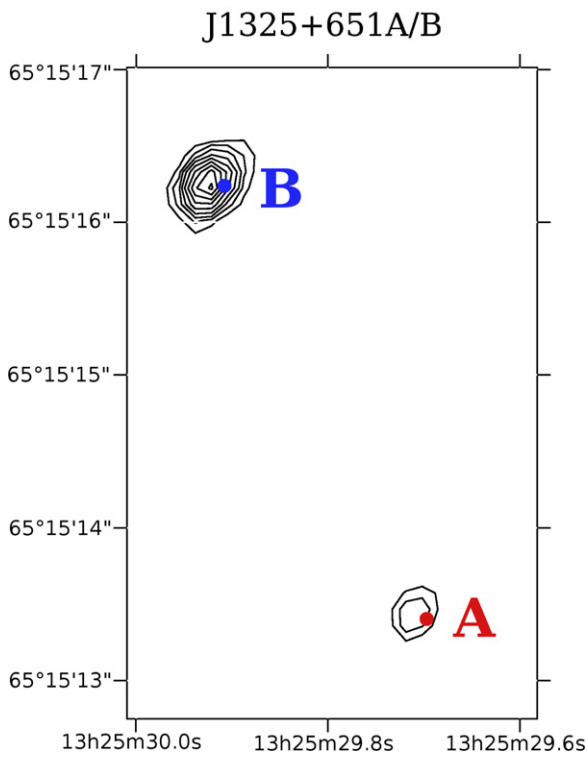

Figure 3. VLA image of double source 1323+65A/1323+65B at 8.4 GHz on epoch 1999 August 8 with beam FWHM 0.″27, project AR415, is shown as a contour map. Although component B is stronger at the VLA image, it is resolved out at the *X* band at VLBA resolution.

(A color version of this figure is available in the online journal.)

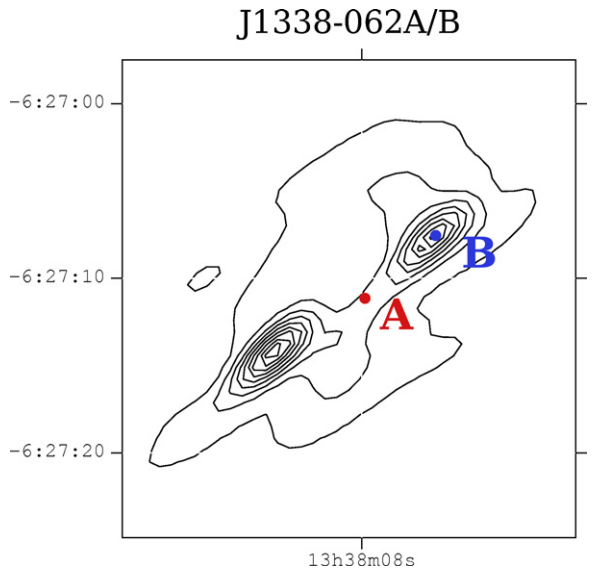

Figure 4. VLA image of double source 1323+65A/1323+65B at 1.4 GHz on epoch 2001 April 29 with beam size 6.″45, project AB950 (FIRST), is shown as a contour map. Component B was detected in OBRS–2 only at the *S* band.

(A color version of this figure is available in the online journal.)

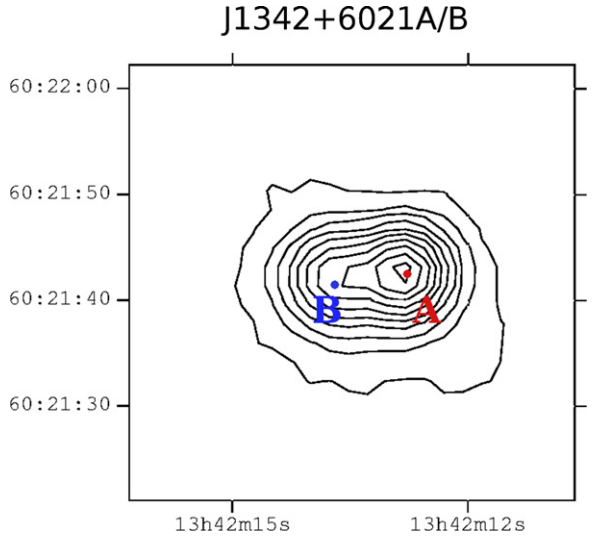

Figure 5. VLA image of double source 1340+60A/1340+60B at 1.4 GHz on epoch 2002 February 7 with beam size 5.″4, project AB950 (FIRST), is shown as a contour map. Component B was detected only at the *S* band.

(A color version of this figure is available in the online journal.)

Component A is within 0.″23 of WISE J134213.26+602142.9, which has magnitude 14.2 at 3.6 μ.

5. DISCUSSION

Position accuracy, 2–5 mas for 80% of OBRS–2 sources, is too coarse to make a meaningful comparison with *Gaia* if the most optimistic estimates of its astrometric performance are realized because the frequency setup of the VLBI observations was not favorable for precise absolute astrometry. With that level of accuracy, we can ignore effects of core shift, which, according to Sokolovsky et al. (2011), have a median value of 0.24 mas at 8 GHz, and ignore the offset between the image peak and the image centroid to which astrometric position is referred.

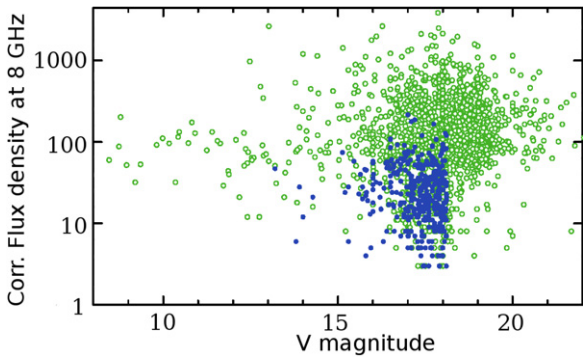

Figure 6. Dependence of the median-correlated flux density at 8 GHz at baselines longer than 5000 km vs. *V* magnitude of those active galactic nuclei that have been detected with VLBI under absolute astrometry programs. Solid blue filled circles show sources detected at the *X* band during the OBRS–1 and OBRS–2 campaigns. Green hollow circles show associated sources observed under other programs.

(A color version and supplemental data of this figure are available in the online journal.)

Cross-referencing the cumulative catalog of radio sources detected with VLBI in the absolute astrometry mode at 8 GHz against the optical catalog of active galactic nuclei, including quasars, of Veron-Cetty & Veron (2010), I found that 1676 objects, or 23%, have a counterpart within a 4″ search radius. Of them, 825 objects are brighter than *V* 18^{m} mag. Of them, 377, or 46%, were observed in OBRS–1 or OBRS–2 programs, and 293 of them were observed only in these two programs. Five OBRS–2 sources, 0012+305, 0232−042, 0744+092, 1146+249, and 1632+198, have position offsets with respect to the optical catalog of quasars in Veron-Cetty & Veron (2010) exceeding 4″. Since their offsets with respect to the *WISE* catalog are in a range of 0.″08–0.″43, I consider that their positions in the optical catalog had an error.

Figure 6 shows the dependence of the correlated flux density versus *V* magnitude for the entire sample of radio–optic associations and for the sub-sample observed in the OBRS–1 and OBRS–2 programs. There is no sign of obvious correlation between optical brightness and radio brightness. We see that the OBRS–1/OBRS–2 sources are systematically weaker than those observed in other programs. Of the 400 sources detected in OBRS–1 and OBRS–2, only 148 have an unresolved component at the *X* band stronger than 30 mJy, while the total number of radio sources associated with quasars brighter than V 18^{m} mag and with an unresolved component stronger than 30 mJy is 683.

If a source is too weak at long baselines, the position uncertainty 0.1 mas will not be achieved within a reasonable integration time because of thermal noise. The median semi-major axis of the position error ellipse of OBRS–1/OBRS–2 sources without reweighting is 2.2 mas. The frequency sequence used in these observing programs results in a group delay uncertainty at a given S/N that is a factor of 11.2 greater than the group delay uncertainty of regular geodetic observations under the RDV program. Even if OBRS programs were observed with the same frequency sequence as RDV experiments, the median position uncertainty due to the thermal noise would have been 0.2 mas. Therefore, future observations for improving source positions associated with optically bright quasars should be focused on observing compact radio sources with a strong unresolved core. *The majority* of such objects were detected in programs *other* than OBRS–1/OBRS–2. Therefore, the OBRS program can only be considered partially successful. Observing sources known as weak from the EVN detection survey (Bourda et al. 2010) was not warranted for the goal of the project. Selection of a frequency sequence that is unfavorable for astrometry degraded position accuracy by one order of magnitude but did not bring any merit.

The VLBI catalog is complete only to flux densities of 180 mJy (Petrov et al. 2013). Figure 6 suggests that other strong radio sources associated with optically bright quasars may exist. Systematic surveys targeted at sources with correlated flux densities at long baselines in a range of 50–180 mJy promise to reveal new radio loud quasars. If we observe each target source for 2 minutes at 512 Mbit s^{-1} at X/S in two scans each with VLBA, ∼1800 sources with correlated flux densities down to 25 mJy could be observed for 242 hr allotted for OBRS–1, OBRS–2, and the EVN detection survey. This approach is an alternative to the strategy adopted for the OBRS project.

6. SUMMARY

Analysis of the second dual-band S/X VLBA campaign of the program for observing optically bright extragalactic radio sources allowed me to determine positions of 295 target sources and make images of 285 of them. Because of the use of a frequency setup unfavorable for absolute astrometry, the position uncertainties ranged from 2 to 200 mas with a median value of 3.2 mas. Many of these sources are suitable as phase calibrators.

This position accuracy is sufficient for using these sources as phase calibrators, but not sufficient for drawing meaningful conclusions from comparisons of *Gaia* and VLBI positions. Approximately, one-third of observed sources have a strong unresolved core, and their positions can be determined with accuracies better than 0.1 mas in future VLBI observing programs with appropriate frequency setup.

The National Radio Astronomy Observatory is a facility of the National Science Foundation operated under cooperative agreement by Associated Universities, Inc. The European VLBI Network is a joint facility of European, Chinese, South African, and other radio astronomy institutes funded by their national research councils. This publication makes use of data products from the *Wide-field Infrared Survey Explorer*, which is a joint project of the University of California, and the JPL/California Institute of Technology, funded by NASA.

Facilities: VLBA (project code GC034), EVN

REFERENCES

Beasley, A. J., Gordon, D., Peck, A. B., et al. 2002, ApJS, 141, 13
Bourda, G., Charlot, P., & Le Campion, J.-F. 2008, A&A, 490, 403
Bourda, G., Charlot, P., Porcas, R. W., & Garrington, S. T. 2010, A&A, 520, 113
Bourda, G., Collioud, A., Charlot, P., Porcas, R. W., & Garrington, S. T. 2011, A&A, 526, A102
Charlot, P., Fey, A. L., Collioud, A., et al. 2007, in Proc. Journées Systèmes de Référence Spatio-temporels 2007, ed. N. Capitaine (Paris: Observatoire de Paris), 8, http://syrte.obspm.fr/jsr/journees2007/pdf/s1_02_Charlot.pdf
Cohen, M. H., & Shaffer, D. B. 1971, AJ, 76, 91
Condon, J., Darling, J., Kovalev, Y. Y., & Petrov, L. 2011, arXiv:1110.6252
Deller, A., Brisken, W. F., Phillips, C. J., et al. 2011, PASP, 123, 275
Fomalont, E., Petrov, L., McMillan, D. S., et al. 2003, AJ, 126, 2562
Kovalev, Y. Y., Lobanov, A. P., Pushkarev, A. B., & Zensus, J. A. 2008, A&A, 483, 759
Kovalev, Y. Y., Petrov, L., Fomalont, E., & Gordon, D. 2007, AJ, 133, 1236
Lanyi, G. E., Boboltz, D. A., Charlot, P., et al. 2010, AJ, 139, 1695

Lindegren, L., Babusiaux, C., Bailer-Jones, C., et al. 2008, in IAU Symp. 248, Giant Step: from Milli- to Micro-arcsecond Astrometry, ed. W. J. Jin, I. Platais, & M. A. C. Perryman (Cambridge: Cambridge Univ. Press), 217
Ma, C., Arias, E. F., Eubanks, T. M., et al. 1998, AJ, 116, 516
Matveenko, L. I., Kardashev, N. S., & Sholomitskii, G. B. 1965, Izvestia VUZov. Radiofizika, 8, 651 (Eng. transl. Sov. Radiophys., 8, 461)
Pearson, T. J., Shepherd, M. C., Taylor, G. B., & Myers, S. T. 1994, BAAS, 26, 1318
Petrov, L. 2011, AJ, 142, 105
Petrov, L., Gordon, D., Gipson, J., et al. 2009, JGeod, 83, 859
Petrov, L., Kovalev, Y. Y., Fomalont, E., & Gordon, D. 2005, AJ, 129, 1163
Petrov, L., Kovalev, Y. Y., Fomalont, E., & Gordon, D. 2006, AJ, 131, 1872
Petrov, L., Kovalev, Y. Y., Fomalont, E., & Gordon, D. 2007, AJ, 136, 580
Petrov, L., Kovalev, Y. Y., Fomalont, E., & Gordon, D. 2011a, AJ, 142, 35
Petrov, L., Mahony, E. K., Edwards, P. G., et al. 2013, MNRAS, 432, 1294
Petrov, L., Phillips, C., Bertarini, A., Murphy, T., & Sadler, E. M. 2011b, MNRAS, 414, 2528
Porcas, R. W. 2009, A&A, 505, L1
Pushkarev, A. B., & Kovalev, Y. Y. 2012, A&A, 544, 34
Shepherd, M. C. 1997, in ASP Conf. Ser. 125, Astronomical Data Analysis Software and Systems VI, ed. G. Hunt & H. E. Payne (San Francisco, CA: ASP), 77
Sokolovsky, K. V., Kovalev, Y. Y., Pushkarev, A. B., & Lobanov, A. P. 2011, A&A, 532, A38
Taylor, G. B., Vermeulen, R. C., Readhead, A. C. S., et al. 1996, ApJS, 107, 37
Veron-Cetty, M. P., & Veron, P. 2010, A&A, 518, A10
Wright, E. L., Eisenhardt, P. R. M., Mainzer, A. K., et al. 2010, AJ, 140, 1868